Chemical Science

EDGE ARTICLE

View Article Online
View Journal | View Issue

Cite this: *Chem. Sci.*, 2018, **9**, 3209

Dual-channel fluorescence diagnosis of cancer cells/tissues assisted by OATP transporters and cysteine/glutathione†‡

Hongxing Zhang,§[a] Jing Liu,§[a] Bo Hu,[b] Linfang Wang,[a] Zhen Yang,[a] Xu Han,[a] Juanjuan Wang,[c] Wei Bai[d] and Wei Guo *[a]

Although fluorescence imaging diagnosis of the differences between cancer cells and normal cells by targeting ligand-based fluorescent probes is useful for recommending personalized therapy to patients, using the differences to diagnose a wide range of cancers is often not possible due to the genetic or phenotypic heterogeneity of cancer cells. In this work a 2-(diphenylphosphino)phenol-functionalized pyronin **POP** was presented as a dual-channel fluorescence agent for diagnosing a wide range of cancer cell types. The agent could efficiently penetrate cancer cell, rather than normal cell, membranes by active transport of the organic-anion transporting polypeptide (OATP) transporters overexpressed in many types of cancer cell, and is then activated by intracellular cysteine (Cys) and glutathione (GSH) to produce green-emission aminopyronin **NP** and red-emission thiopyronin **SP**, thereby enabling its use in dual-channel fluorescence diagnosis of a wide range of cancer cells with excellent contrast. Crucially, **POP** also displays the ability of dual-channel fluorescence diagnosis of cancer tissues from tumour xenograft models of mice and harvested surgical specimens of patients, thus holding great potential for clinical applications.

Received 21st December 2017
Accepted 15th February 2018

DOI: 10.1039/c7sc05407f

rsc.li/chemical-science

Introduction

Discrimination of cancer cells/tissues from normal cells/tissues is of critical importance for the early diagnosis and treatment of cancers. Currently, the common methods for tumour diagnosis include cyto- or histopathological examination of biopsies, magnetic resonance imaging, positron emission tomography, single-photon emission computed tomography and X-ray imaging. However, these techniques do not often work well until the middle to late stages, when metastasis and diffusion have occurred, due to the lack of sufficient specificity and sensitivity; moreover, some of them suffer from radiological hazards.[1] By comparison, fluorescence probe-based imaging techniques offer the exciting opportunity to overcome these limitations in terms of their high-sensitivity, visualization, non-invasiveness, absence of ionizing radiation and real-time imaging ability *in vivo* even at the single living cell level.[2] To enhance the specificity, in addition to utilizing the conventional enhanced permeation and retention (EPR) effect,[3] the most common strategy for such probes is chemical conjugation of fluorophores with targeting ligands, including chemical molecules, peptides, proteins, antibodies and aptamers, which could specifically bind to the biomarkers overexpressed in cancer cells.[2,4,5] However, although fluorescence imaging diagnosis of the differences between cancer cells and normal cells by such probes is useful for recommending personalized therapy to patients, using the differences to diagnose a wide range of cancers is often not possible due to the genetic or phenotypic heterogeneity of cancer cells. Thus, some efforts have also focused on deregulated tumour metabolism, *i.e.* aerobic glycolysis (also known as the Warburg effect),[6] which creates a cancer-specific microenvironment with conditions such as decreased extracellular pH[7] and enhanced levels of reactive oxygen species (ROS).[8,9] However, only a limited amount of examples of success have been achieved using this strategy to date.[10–15] Recently, a class of near-infrared (NIR) heptamethine cyanine dyes were reported to be able to accumulate preferentially in a wide range of cancer cell types without the need for chemical conjugation to tumour targeting ligands.[16–20] Further studies revealed that organic-anion transporting polypeptide (OATP) transporters, overexpressed in many types of cancer cell[21,22] and well-recognized as channels for a diverse group of substrates,[23] play the dominant roles[17] and open up new

[a]*School of Chemistry and Chemical Engineering, Shanxi University, Taiyuan 030006, China. E-mail: guow@sxu.edu.cn*
[b]*China Institute for Radiation Protection, Taiyuan 030006, China*
[c]*Scientific Instrument Center, Shanxi University, Taiyuan 030006, China*
[d]*Shanxi Provincial Cancer Hospital, Taiyuan 030013, China*

† Dedicated to Prof. Jin-Pei Cheng on the occasion of his 70th birthday.

‡ Electronic supplementary information (ESI) available: Synthesis, experimental procedures, supplemental spectra and imaging data and ^{1}H-, ^{13}C-NMR and MS spectra. See DOI: 10.1039/c7sc05407f

§ These authors contributed equally to this work.

possibilities for the design of broad-spectrum fluorescence agents to target cancer cells/tissues. However, despite their successful applications in *in vivo* imaging of tumours, these cyanine dyes require a long time to achieve an adequate signal-to-background ratio due to their "always-on" fluorescence feature. All in all, the discovery of a new molecular system for efficiently discriminating a wide range of cancer cells from normal cells represents an urgent and essential diagnosis need. Herein, we describe our work in this regard.

We previously reported a 4-methoxythiophenol-functionalized pyronin dye[24] which is capable of simultaneous fluorescence imaging of cysteine (Cys) and glutathione (GSH) from green and red channels based on a Cys-induced substitution-rearrangement reaction and a GSH-induced substitution reaction. We envisioned that this dye may have the potential to discriminate cancer cells from normal cells in terms of the elevated levels of GSH in many types of cancer cell for resisting intrinsic oxidative stress.[25] However, subsequent imaging assays disproved the hypothesis, because the dye could penetrate both the cancer and normal cell membranes and react with intracellular Cys and GSH to give bright fluorescence in green and red channels (Fig. S1, ESI‡). We initially speculated that the high reactivity of the dye may lead to its failure in differentiating the different biothiol levels between cancer cells and normal cells. Thus, we synthesized a phenol-functionalized pyronin **OP** (ESI‡) (Scheme 1A) in the hope that the phenoxy group with poor leaving ability may be less efficient for the low concentration of biothiols in normal cells, but active enough for the higher concentration of biothiols in cancer cells. Regrettably, **OP** was found to be inert toward Cys/GSH in the simulated physiological conditions (Fig. S2, ESI‡). Considering that the poorly basic triphenylphosphine group has the possibility of enhancing the reactivity of Cys/GSH by synergistically deprotonating their –SH group in the reaction transition state (Fig. S3, ESI‡), a 2-(diphenylphosphino)phenol-functionalized pyronin **POP** was further synthesized (ESI‡). Surprisingly, **POP** could not only react with Cys and GSH to produce green-emission aminopyronin (**NP**) and red-emission thiopyronin (**SP**) in the simulated physiological conditions (Scheme 1A), but could also preferentially accumulate in cancer cells, rather than normal cells, by OATP-mediated active transport, and then light them up from both green and red channels by reacting with the abundant intracellular Cys/GSH (Scheme 1B). Thereby, a wide range of cancer cell types could be rapidly diagnosed using the dual-channel mode with excellent contrast. Importantly, **POP** displays the ability of simultaneous dual-channel fluorescence diagnosis of cancer tissues from both tumour xenograft models of mice and harvested surgical specimens of patients, thus holding great potential for the clinical diagnosis of human cancer. The detailed results are illustrated as follows.

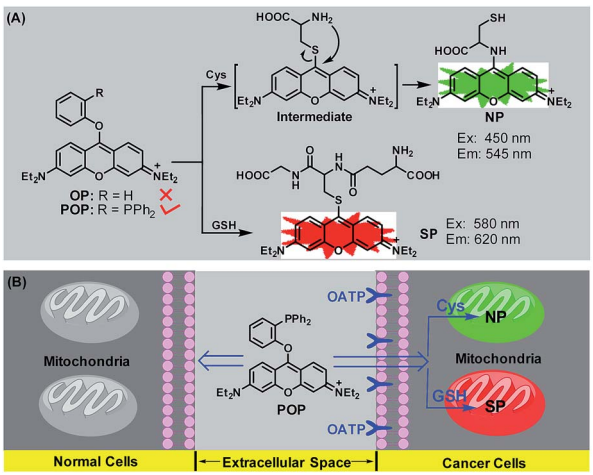

Scheme 1 (A) Sensing mechanisms of **POP** for Cys and GSH. (B) Schematic illustration of the dual-channel fluorescence discrimination of cancer cells from normal cells by **POP**.

Results and discussion

Spectral response of POP for Cys and GSH

As shown in Fig. S4 ESI,‡ **POP** showed a main absorption peak at 545 nm in PBS (10 mM, pH = 7.4, 37 °C) and this remained stable in the time range of 0–60 min; upon separate treatments with Cys and GSH, a new blue-shift peak at 455 nm for the former and a new red-shift peak at 593 nm for the latter were observed. According to the well-established reaction mechanisms reported by us previously,[24,26] the peaks at 455 nm and 593 nm could be assigned to aminopyronin **NP** and thiopyronin **SP**, respectively. This could be further supported by HRMS studies, where the corresponding molecular ion peaks of **NP** and **SP** could clearly be observed (Fig. S5, ESI‡). The fluorescence response of **POP** for Cys and GSH was subsequently tested using two different excitation wavelengths at 450 nm and 580 nm, which are close to the absorption maxima of **NP** and **SP**, respectively. As shown in Fig. 1A and B, it was found that whether excited at 450 nm or at 580 nm **POP** showed a poor fluorescence background, although it displayed an obvious fluorescence signal at 570 nm when excited at 520 nm (near the absorption maximum of **POP**) (Fig. S6, ESI‡); however, when Cys and GSH were separately added to the **POP** solution, a big fluorescence enhancement (λ_{em} = 545 nm for the former and λ_{em} = 620 nm for the latter) could be observed within 6 min in both cases, in line with the production of green-emission **NP** and red-emission thiopyronin **SP**.[24,26] Further, fluorescence titration studies revealed that the maximal fluorescence responses could be obtained when 100 equiv. of Cys and 5 equiv. of GSH were used (Fig. S7, ESI‡) indicating that the physiological concentrations of Cys and GSH should be able to elicit an adequate fluorescence response from **POP** in green and red channels. Moreover, the fluorescence spectra caused by Cys and GSH had negligible overlap, indicating that **POP** could efficiently discriminate the two biothiols from green and red channels. In contrast, when the **POP** solution was treated with various amino acids, reducing agents, metal ions and reactive oxygen/nitrogen species (ROS/RNS), only negligible fluorescence changes in both green and red channels were observed (Fig. 1C and D), confirming the high selectivity of **POP** for Cys and GSH, respectively.

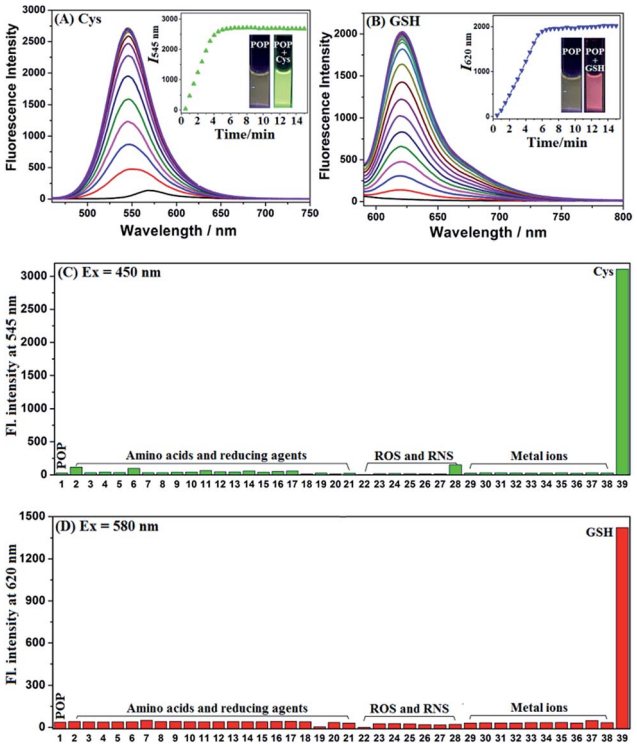

Fig. 1 (A and B) Time-dependent fluorescence spectra changes of **POP** (2 μM) upon treatment with Cys (100 equiv.) and GSH (10 equiv.), respectively, in PBS (10 mM, pH 7.4) at 37 °C. (C and D) Fluorescence intensity changes of **POP** (2 μM) treated with various amino acids (200 μM), reducing agents (200 μM), ROS (100 μM) and metal ions (500 μM). (1) **POP**; (2) His; (3) Glu; (4) Asp; (5) Val; (6) Phe; (7) Tyr; (8) Ala; (9) Ser; (10) Leu; (11) Arg; (12) Pro; (13) Thr; (14) Glu; (15) Trp; (16) Ile; (17) Lys; (18) DTT; (19) Vc; (20) HS^- for (C) and Cys for (D); (21) GSH for (C) and HS^- for (D); (22) $ONOO^-$; (23) H_2O_2; (24) NaOCl; (25)$OH^•$; (26) KO_2; (27) NO; (28) HNO; (29) K^+; (30) Ca^{2+}; (31) Na^+; (32) Mg^{2+}; (33) Al^{3+}; (34) Zn^{2+}; (35) Cd^{2+}; (36) Cu^{2+}; (37) Fe^{2+}; (38) Fe^{3+}; (39) Cys for (C) and GSH for (D). For (A and C) $\lambda_{ex} = 450$ nm; for (B and D) $\lambda_{ex} = 580$ nm. Slits: 5/5 nm.

Dual-channel fluorescence discrimination of cancer cells from normal cells using POP

Prior to bioimaging assays, CCK8 assays were performed to check the cytotoxicity of **POP** in human cervix carcinoma HeLa cells. As shown in Fig. S8 ESI,‡ HeLa cells treated with various concentrations of **POP** (0–10 μM) for 24 h showed high cell viability (~100%), indicating that the agent has fairly low toxicity to living cells. Following this favourable toxicity assessment the ability of **POP** for simultaneous dual-channel fluorescence imaging of Cys and GSH in HeLa cells was tested. As shown in Fig. S9 ESI,‡ **POP** was found to be able to rapidly penetrate HeLa cell membranes (within 30 min) to give bright intracellular fluorescence in both green and red channels. Moreover, when the cells were pre-treated with exogenous Cys (or GSH) and then treated with **POP**, the stronger fluorescence signal could be observed in the green channel (or red channel); when the cells were pre-treated with 0.5 mM H_2O_2 (an oxidizing agent for biothiols) or 1 mM *N*-ethylmaleimide (NEM, a trapping reagent for biothiols) and then treated with **POP**, the intracellular fluorescence in the two channels both greatly decreased (Fig. S10, ESI‡). These results, coupled with those observed in the chemical system, indicate that **POP** is capable of simultaneous dual-channel fluorescence imaging of Cys and GSH in the cellular environment. Also, we performed co-staining assays to evaluate the subcellular localization of **POP** and its reaction products **NP** and **SP**. As shown in Fig. S11 ESI,‡ the obtained results revealed that these compounds could all preferentially localize in the mitochondria, consistent with their electropositive pyronin core which could direct them into the mitochondria due to the highly negative mitochondrial membrane potentials.[27] In addition, it should be mentioned that due to the structural similarity between Cys and homocysteine (Hcy), **POP** also showed similar spectral responses for Hcy (Fig. S12, ESI‡). Thus, Hcy should also make a contribution to the intracellular green fluorescence observed in the above assays, although the contribution is insignificant because the cellular Hcy concentration (*ca.* 10 μM) is much lower than that of Cys (*ca.* 0.2 mM) or GSH (*ca.* 5 mM).

With intense curiosity, we further tested whether **POP** could discriminate cancer cells from normal cells in terms of the higher biothiol levels in cancer cells.[25] To our delight, as shown in Fig. 2, when cancer cells, including A549 cells, HeLa cells, MCF-7 cells, SMMC-7721 cells and HepG2 cells, were treated with **POP** for 30 min, all of them could be lit up in both green and red channels; in sharp contrast, when the same procedure was applied to normal cells including BRL-3A cells, HUVECs cells, RASMC cells, SHEE cells, MSC cells and COS-7 cells,

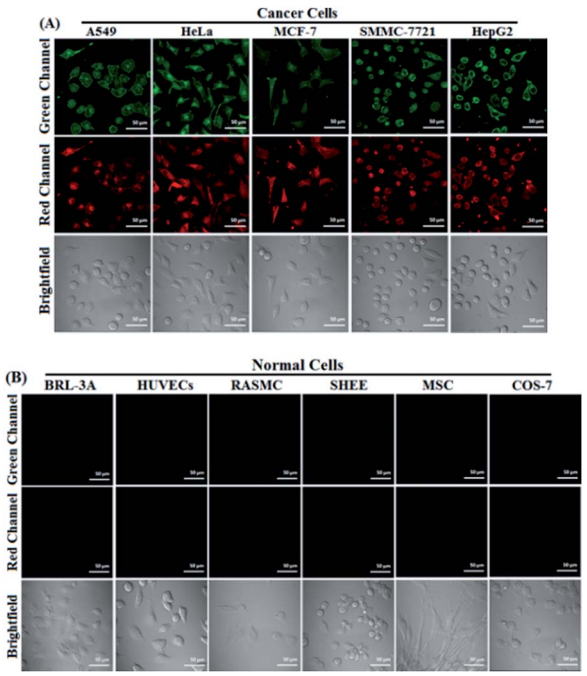

Fig. 2 Confocal fluorescence images of cancer cells (A) and normal cells (B) treated with **POP** (4 μM, 30 min). For the green channel, the emission was collected at 500–540 nm ($\lambda_{ex} = 488$ nm); for the red channel, the emission was collected at 650–700 nm ($\lambda_{ex} = 561$ nm). Scale bar: 50 μm.

almost no intracellular fluorescence was observed in the two channels. These results, although positive, are considerably surprising, because the physiological concentrations of Cys and GSH in normal cells should be high enough to elicit the obvious fluorescence response of **POP**, as was the case for the 4-methoxythiophenol-functionalized pyronin mentioned before (Fig. S1, ESI‡).[24] Thus, the difference in biothiol levels between cancer cells and normal cells should not be the determining factor for the above observed excellent imaging contrast. Furthermore, it was found that when normal COS-7 cells were pre-treated with **POP** for 30 min and then treated with exogenous Cys or GSH for another 30 min, the intracellular fluorescence was not yet observed in both green and red channels (Fig. S13, ESI‡), thus precluding the possibility that the negligible fluorescence observed in normal cells is due to their low biothiol levels. Based on these results, it was concluded that **POP** could efficiently penetrate cancer cell membranes, rather than normal cell membranes, and then react with intracellular Cys and GSH to give fluorescence in both green and red channels.

Uptake mechanism of POP by cancer cells

Encouraged by these results, we then studied the possible uptake mechanism of **POP** by cancer cells. Firstly, a comparison study of cellular uptake was carried out at 37 °C and 4 °C. As shown in Fig. 3, HeLa cells incubated with **POP** at 4 °C for 30 min showed obviously decreased intracellular fluorescence compared to that obtained at 37 °C, indicating that the cellular uptake of **POP** is energy-dependent. This speculation could further be supported by inhibition assays, where 2-deoxy-D-glucose (2-DG, an inhibitor of glycolysis preferentially utilized by cancer cells for energy supply), rather than oligomycin (an inhibitor of oxidation phosphorylation utilized by normal cells for energy supply), was found to substantially lower the cellular uptake of **POP** (Fig. 3).[16,17] Furthermore, we studied the possible pathways that control the energy-dependent intake of molecules by cells, *i.e.* cellular endocytosis and direct translocation by transporters. As shown in Fig. 4, it was found that various endocytotic inhibitors, including chlorpromazine (clathrin inhibitor), amiloride (actin inhibitor) and methyl-β-cyclodextrin (MβCD, caveolae inhibitor),[16] did not obviously affect the intracellular fluorescence intensities of **POP**, suggesting that the cellular uptake of **POP** was not mediated by an endocytotic mechanism. However, when HeLa cells were pre-treated with sulfobromophthalein (BSP), a competitive inhibitor of OATP transporters,[16,17,28] and then treated with **POP**, the cellular fluorescence was almost completely inhibited (Fig. 4), strongly indicating that **POP** uptake by cancer cells is actively mediated by OATP transporters, which are overexpressed in a variety of cancer cells[21,22] and capable of membrane transport of many substrates including cationic compounds.[23] Taken together, the observed energy-dependence of cellular **POP** uptake as well as the OATP-mediated active transport strongly indicate that it would be difficult for **POP** to penetrate normal cell membranes by common energy-independent passive diffusion, but easy to penetrate cancer cell membranes assisted by OATP transporters. As for why the aforementioned 4-methoxythiophenol-functionalized pyronin[24] could penetrate both cancer and normal cell membranes, this could reasonably be attributed to the different cellular uptake mechanism, *i.e.* energy-independent passive diffusion, as indicated by its strong cell penetration ability for cancer and normal cells (Fig. S1, ESI‡).

Dual-channel fluorescence diagnosis of cancer tissues using POP

Following confirmation that **POP** successfully discriminates cancer cells from normal cells, its potential for diagnosing cancer tissues was further explored. Tumour-bearing nude mice were prepared by subcutaneous injection of A549 or HepG2 cells into the left axillae of the nude mice. The mice were then sacrificed and various tissues, including tumour, heart, liver, spleen, lung and kidney, were cryo-sectioned as 20 μm thicknesses. After being washed with PBS three times these slices were treated with **POP** (4 μM) for 20 min in PBS, followed by

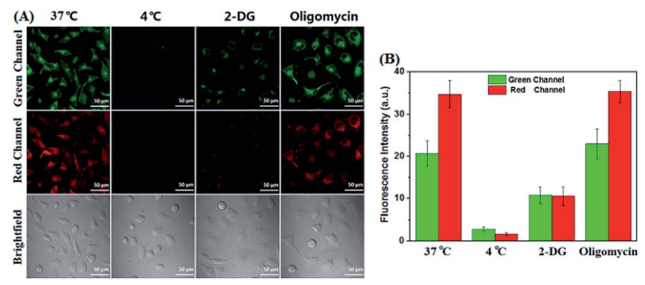

Fig. 3 (A) Confocal fluorescence images of HeLa cells incubated with **POP** (4 μM, 30 min) in PBS at 37 °C and 4 °C, or pre-treated with 2-DG (150 mM, 45 min) and oligomycin (5 μM, 45 min) in DMEM at 37 °C and then treated with **POP** (4 μM, 30 min) in PBS at 37 °C after being washed with PBS three times. (B) Average fluorescence intensities from the images shown in (A). For the green channel, the emission was collected at 500–540 nm (λ_{ex} = 488 nm); for the red channel, the emission was collected at 650–700 nm (λ_{ex} = 561 nm). Scale bar: 50 μm.

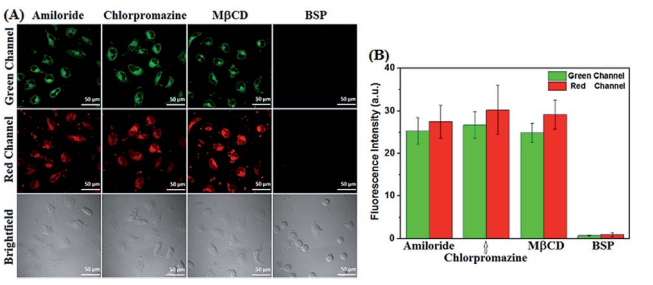

Fig. 4 (A) Confocal fluorescence images of HeLa cells pre-treated with various endocytotic inhibitors [amiloride (20 μg mL^{-1}, 30 min), chlorpromazine (10 μg mL^{-1}, 30 min) and MβCD (7.5 mM, 30 min)] and OATP inhibitor BSP (250 μM, 5 min) in DMEM and then treated with **POP** (4 μM) in PBS for 30 min at 37 °C after being washed with PBS three times. (B) Average fluorescence intensities from images shown in (A). For the green channel, the emission was collected at 500–540 nm (λ_{ex} = 488 nm); for the red channel, the emission was collected at 650–700 nm (λ_{ex} = 561 nm). Scale bar: 50 μm.

imaging using confocal microscopy. As shown in Fig. 5A and S14 ESI,‡ the strong fluorescence from both green and red channels could be clearly observed only in the tumour tissues, whereas the normal tissues, including heart, liver, spleen, lung and kidney, all showed negligible fluorescence in the two channels. Thus, **POP** could also be utilized to discriminate cancer tissue from normal tissue. Furthermore, **POP** was used to diagnose human cancer tissue. In the assays, human lung, thyroid and ovarian cancer tissues and human ovarian and cervical normal tissues, harvested from surgical specimens of patients and determined by doctors, were cryo-sectioned as 5 μm thicknesses and then treated with the same procedure mentioned above. As shown in Fig. 5B, these cancer tissues, as expected, all showed strong fluorescence in both green and red channels, whereas the normal tissues displayed minor or negligible fluorescence in the two channels, indicating the potential of **POP** for clinical diagnosis of human cancers. Note that before **POP** treatment in the above assays, it is necessary to thoroughly wash these slices with PBS; otherwise, some background fluorescence caused by the biothiol in blood was also observed in normal tissues, as indicated by the similar spectra changes of the probe treated with fetal bovine serum (FBS) compared to that treated with Cys (Fig. S15, ESI‡).

Conclusions

In summary, a 2-(diphenylphosphino)phenol-functionalized pyronin **POP** has been presented as a dual-channel fluorescence agent for diagnosing cancer cells and tissues. The agent could rapidly penetrate cancer cell, rather than normal cell, membranes by active transport of organic-anion transporting polypeptide transporters overexpressed in many types of cancer cell, and then is activated by the abundant intracellular Cys and GSH to produce green-emission aminopyronin and red-emission thiopyronin, thereby enabling its use in dual-channel fluorescence diagnosis of a wide range of cancer cells with excellent contrast. The practical applications of this agent for the dual-channel fluorescence diagnosis of tumour tissues, harvested from both tumour xenograft models of mice and surgical specimens of patients, have also been successfully realized. Currently, the agent is being applied in further diagnoses of human cancers from harvested surgical specimens of patients.

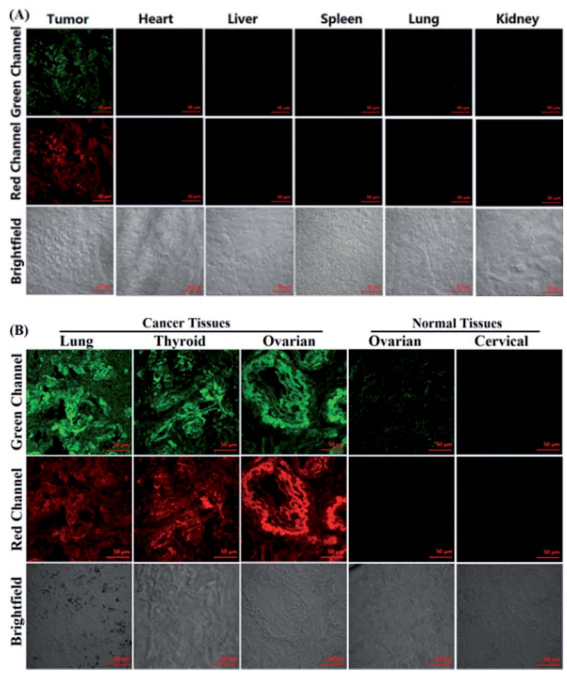

Fig. 5 Confocal fluorescence images of **POP** (4 μM) stained cancer and normal tissue cryosections from an A549 xenograft nude mouse model (A) and five harvested surgical specimens of patients (B). Scale bar: 50 μm.

Conflicts of interest

There are no conflicts to declare.

Acknowledgements

This work was supported by the Natural Science Foundation of China (No. 21572121, 21502108 and 21302114), Natural Science Foundation for Youth of Shanxi (No. 201601D021055), Scientific and Technological Innovation Programs of Higher Education Institutions in Shanxi and Scientific Instrument Center of Shanxi University. The assays were performed in compliance with the relevant laws and institutional guidelines and animal care and handling procedures were reviewed and approved by the Animal Care and Use Committee of Shanxi University. The harvested surgical specimens of patients, including human lung, thyroid and ovarian cancer tissues as well as human ovarian and cervical normal tissues, were obtained from Shanxi Provincial Cancer Hospital. Informed consent was obtained for any experimentation with human subjects.

Notes and references

1 L. Fass, *Mol. Oncol.*, 2008, **2**, 115–152.
2 M. Gao, F. Yu, C. Lv, J. Choo and L. Chen, *Chem. Soc. Rev.*, 2017, **46**, 2237–2271.
3 H. Maeda, J. Wu, T. Sawa, Y. Matsumura and K. Hori, *J. Controlled Release*, 2000, **65**, 271–284.
4 Y. Urano, M. Sakabe, N. Kosaka, M. Ogawa, M. Mitsunaga, D. Asanuma, M. Kamiya, M. R. Young, T. Nagano, P. L. Choyke and H. Kobayashi, *Sci. Transl. Med.*, 2011, **3**, 110–119.
5 M. Chiba, Y. Ichikawa, M. Kamiya, T. Komatsu, T. Ueno, K. Hanaoka, T. Nagano, N. Lange and Y. Urano, *Angew. Chem., Int. Ed.*, 2017, **56**, 10418–10422.
6 M. G. V. Heiden, L. C. Cantley and C. B. Thompson, *Science*, 2009, **324**, 1029–1033.
7 B. A. Webb, M. Chimenti, M. P. Jacobson and D. L. Barber, *Nat. Rev. Cancer*, 2011, **11**, 671–677.
8 F. Antunes and E. Cadenas, *Free Radical Biol. Med.*, 2001, **30**, 1008–1018.

9 T. P. Szatrowski and C. F. Nathan, *Cancer Res.*, 1991, **51**, 794–798.
10 T. Zhao, G. Huang, Y. Li, S. Yang, S. Ramezani, Z. Lin, Y. Wang, X. Ma, Z. Zeng, M. Luo, E. de Boer, X.-J. Xie, J. Thibodeaux, R. A. Brekken, X. Sun, B. D. Sumer and J. Gao, *Nat. Biomed. Eng.*, 2006, **1**, 0006.
11 X. Wu, Y. Tian, M. Yu, J. Han and S. Han, *Biomater. Sci.*, 2014, **2**, 972–979.
12 D.-D. He, W. Liu, R. Sun, C. Fan, Y.-J. Xu and J.-F. Ge, *Anal. Chem.*, 2015, **87**, 1499–1502.
13 X. Wu, M. Yu, B. Lin, H. Xing, J. Han and S. Han, *Chem. Sci.*, 2015, **6**, 798–803.
14 H. Zhu, J. Fan, J. Wang, H. Mu and X. Peng, *J. Am. Chem. Soc.*, 2014, **136**, 12820–12823.
15 H. Zhang, J. Liu, C. Liu, P. Yu, M. Sun, X. Yan, J.-P. Guo and W. Guo, *Biomaterials*, 2017, **133**, 60–69.
16 S. Luo, X. Tan, S. Fang, Y. Wang, T. Liu, X. Wang, Y. Yuan, H. Sun, Q. Qi and C. Shi, *Adv. Funct. Mater.*, 2016, **26**, 2826–2835.
17 E. Zhang, S. Luo, X. Tan and C. Shi, *Biomaterials*, 2014, **35**, 771–778.
18 S. Luo, X. Tan, Q. Qi, Q. Guo, X. Ran, L. Zhang, E. Zhang, Y. Liang, L. Weng, H. Zheng, T. Cheng, Y. Su and C. Shi, *Biomaterials*, 2013, **34**, 2244–2251.
19 X. Tan, S. Luo, D. Wang, Y. Su, T. Cheng and C. Shi, *Biomaterials*, 2012, **33**, 2230–2239.
20 S. Luo, E. Zhang, Y. Su, T. Cheng and C. Shi, *Biomaterials*, 2011, **32**, 7127–7138.
21 N. Thakkar, A. C. Lockhart and W. Lee, *AAPS J.*, 2015, **17**, 535–545.
22 T. Nakanishi and I. Tamai, *Biopharm. Drug Dispos.*, 2014, **35**, 463–484.
23 C. Marzolini, R. G. Tirona and R. B. Kim, *Pharmacogenomics*, 2004, **5**, 273–282.
24 J. Liu, Y.-Q. Sun, H. Zhang, Y. Huo, Y. Shi and W. Guo, *Chem. Sci.*, 2014, **5**, 3183–3188.
25 M. P. Gamcsik, M. S. Kasibhatla, S. D. Teeter and O. M. Colvin, *Biomarkers*, 2012, **17**, 671–691.
26 Y.-Q. Sun, J. Liu, H. Zhang, Y. Huo, X. Lv, Y. Shi and W. Guo, *J. Am. Chem. Soc.*, 2014, **136**, 12520–12523.
27 Z. Xu and L. Xu, *Chem. Commun.*, 2016, **52**, 1094–1119.
28 Y. Cui, J. Konig, I. Leier, U. Buchholz and D. Keppler, *J. Biol. Chem.*, 2001, **276**, 9626–9630.